GEOPHYSICS, VOL. 46, NO. 2 (FEBRUARY 1981); P. 152–162, 10 FIGS.

# Linear inversion of body wave data—Part II: Attenuation versus depth using spectral ratios

R. S. Jacobson,* George G. Shor, Jr.,‡ and LeRoy M. Dorman‡


## ABSTRACT

We present a method for determining the specific quality factor $Q^{-1}$ by the use of spectral ratios of seismic refraction data. The only modifications to standard refraction profiles are that the source and receivers be sufficiently far away from reflective boundaries to eliminate the angular dependence of the source spectrum itself and of the observation of the source signal by the receiver. The last requirement may not be too significant. Application of this method for determining attenuation as a function of depth was applied to data obtained in a thick sedimentary section in the Bay of Bengal. Once an adequate velocity-depth function is determined, attenuation as a function of depth is readily calculated by the use of linear inverse theory. Several preferred solutions are discussed, including a model of constant $Q^{-1}$ of 0.0115. A comparison of our data with a compilation of data from the published literature of attenuation with depth reveals a reasonable concordance, but with some slight differences. A peak of attenuation at 600-m depth probably represents the depth of lithification of the sediments into mudstone.


## INTRODUCTION

Although marine seismic refraction profiles have been undertaken in the past 50 years primarily to elucidate velocity structures, relatively little attention has been paid to measuring attenuation. Attenuation measurements, in conjunction with velocity, can add more information to our inferences of the composition and properties of the earth. Unfortunately, since we cannot place sensors deep within the earth, we cannot directly measure intrinsic attenuation, that absorption due to frictional heating, viscous losses, etc. The absorption that we can observe is called "effective" attenuation, and includes (along with intrinsic attenuation) losses due to scattering, reflections, interbed multiples, shear-wave conversions, etc., but it should not include spreading losses. It is plain that structure, velocity contrasts, and the geometry of the observations can alter the value of effective attenuation, even though intrinsic attenuation remains constant. All is not lost, though, for most measurements show a remarkable concordance, at least in marine sediments, so that some conclusions can be drawn.

A compilation of compressional wave attenuation coefficients, gathered from the published literature (Hamilton, 1976a) in unlithified marine sediments, suggests a peak of attenuation at 200-m depth. Hamilton's speculation about this phenomenon was that the effect of porosity reduction due to burial increases attenuation, while pressure effects on the frame structure of the sediments cause a decrease of attenuation. The two effects counterbalance each other at about 200-m depth. At greater depths, further reductions of porosity are small, so overburden pressure on the sediments dominate to produce a reduction in attenuation. As noted by Hamilton, however, no single experiment has possessed the resolution to describe the value of the attenuation peak or its depth. A recent experiment (Mitchell and Focke, 1980) verifies the existence of a peak in attenuation at 250-m depth in one profile, but they report values of attenuation lower than that which Hamilton predicts by an order of magnitude.

We present results of an attenuation measurement experiment which has the necessary resolution to verify Hamilton's predictions. We first outline the method, by using spectral ratios, to determine attenuation values. This method is derived from amplitude observations, and it is similar to the approach taken by Dorman (1968). We then discuss how the data were collected. As we shall see, attenuation measurements are intimately associated with velocity structure, so a discussion of the velocity-depth profile is in order. Finally, the results of the attenuation depth profile are discussed.

## DERIVATION OF SPECTRAL RATIOS

Acoustic energy traveling through a region of vertically heterogeneous, but laterally homogenous, structure is a function of frequency $f$, depth of penetration $z$, and angle of incidence from the vertical $\theta$. More explicitly, the spectrum of the amplitude of the received signal waveform can be described as follows:

$$A_j(\theta, f, z) = E_{0j}(\theta, f)F_j(\theta, f, z)I(f), \qquad (1)$$

where $A$ is the received signal, $E_0$ is the source signal, $F$ is the earth response, and $I$ is the instrument response. Index $j$ specifies each observation of refracted energy, which penetrates to a different depth in the earth. All information about the earth is contained in the functional $F$, which can be further described as

Manuscript received by the Editor May 1, 1980; revised manuscript received June 17, 1980.
*Formerly University of California, San Diego, Scripps Institution of Oceanography; presently Naval Ocean Research and Development Activities, Code 362, NSTL Station, Bay St. Louis, MS 39529.
‡University of California, San Diego, Scripps Institution of Oceanography, La Jolla, CA 92093.
0016-8033/81/0201—152$03.00. © 1981 Society of Exploration Geophysicists. All rights reserved.



Downloaded 23 Feb 2012 to 134.246.166.168. Redistribution subject to SEG license or copyright; see Terms of Use at http://segdl.org/

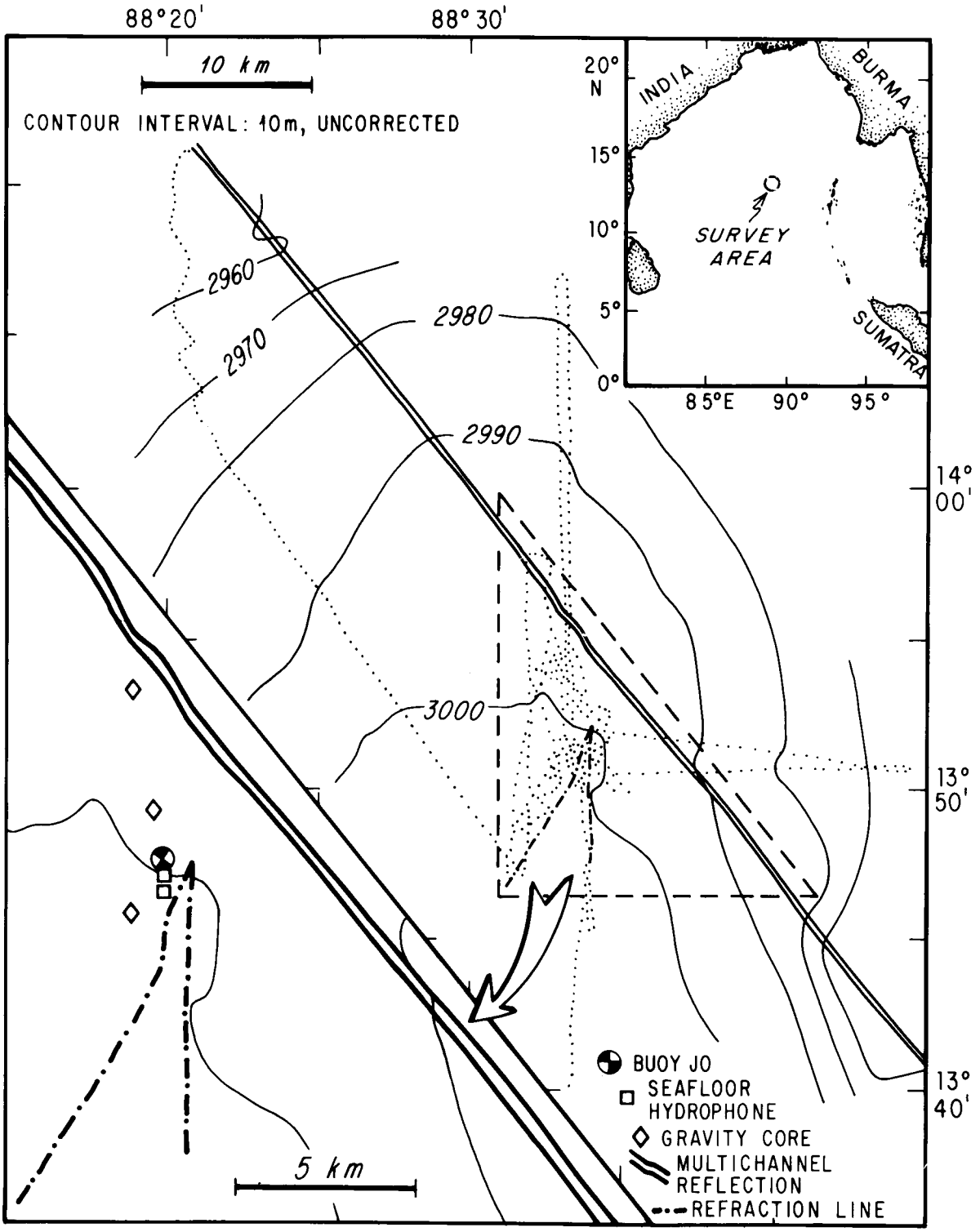


FIG. 1. Bathymetric map of the seismic refraction station in the central Bay of Bengal, detailing the locations of the seismic runs, sea floor hydrophones, the moored buoy (Buoy Jo) and gravity cores, and the multichannel reflection line.

Downloaded 23 Feb 2012 to 134.246.166.168. Redistribution subject to SEG license or copyright; see Terms of Use at http://segdl.org/

$$F_j(\theta, f, z) = T_j(\theta, z) R_j(\theta, z) G_j(f, z), \quad (2)$$

where $T$ is the function containing reflection and transmission coefficients (which we assume to be independent of frequency), scattering losses, conversions to shear waves, etc., $R$ is the spreading loss function, and $G$ is the attenuation operator. $G$ is commonly expressed as

$$G(f, z) = \exp\left(\frac{\pi f t}{-Q(f, z)}\right), \quad (3)$$

where $t$ is the traveltime spent in the attenuating medium. The well-known specific quality factor $Q^{-1}$ is the attenuation depth function we seek. Although $Q^{-1}$ is a dimensionless quantity, its units can be expressed as nepers/radian. A neper is the analog of a decibel; one neper is equal to 8.686 dB. We now assume that $Q$ is independent of frequency, and later we provide justification for doing so.

Another method of describing $G$, used by Hamilton (1972, 1976a), is

$$G(f, z) = \exp\left[-k(z) f^n PL(z)\right], \quad (4)$$

where $k$ is the attenuation coefficient, measured in dB/Hz/km or dB/kHz/m, and $PL$ is the path length. It should be noted that $Q^{-1}$ and $k$ are not directly equivalent. This will be brought up again. Hamilton (1972) observed that the attenuation coefficient in marine sediments appears to be independent of frequency in the range from a few hertz to the megahertz range, and thus assumes that $n$ is equal to unity. This is equivalent to taking $Q^{-1}$ to be independent of frequency. The attenuation coefficient is a useful value in determining sediment types and is also helpful in intercomparisons of sediment properties.

It should also be noted that a frequency-independent $Q^{-1}$ implies a dispersionless medium. Hard rock studies clearly indicate a frequency-dependent $Q^{-1}$ (Jeffreys, 1965) to account for the observed physical dispersion of surface waves and free oscillations. Hamilton (1972) discusses dispersion in marine sediments and concludes it is a neglible effect.

Assuming the instrument response is known, and an accurate measure of the source function is known, we can then solve for the earth response $F$ knowing our received signal. One measure of the source function is from that of the direct waterborne signal. A complexity arises in the source signal from reflections from surfaces that introduce an angular dependence upon its frequency characteristics. If the source and receiver are far enough away from reflective boundaries, this problem is eliminated, and the source function becomes independent of inclination. Also, water does not significantly absorb acoustic energy in the seismic band (Urick, 1975). Each observation of the direct waterborne path can be expressed as

$$A_{wj}(\theta, f, z_w) = E_0(f) R_{wj}(\theta, z_w) I(f), \quad (5)$$

where $R$ represents geometrical spreading losses through the water column and $wj$ indexes each $j$th observation through the water. Thus, our observation of the direct water path immediately yields an excellent source spectrum, offset in absolute levels by spreading losses. If one needs to know exactly, adjustments can be made for accurate source levels by considering spreading losses and instrument response.

Once we know the spectrum of the source, we can divide it into the spectrum of the received energy to give us a spectral ratio, i.e.,

$$\frac{A_j(\theta, f, z)}{A_{wj}(\theta, f, z_w)} = \frac{T_j(\theta, z) R_j(\theta, z) G_j(f, z)}{R_{wj}(\theta, z_w)} \quad (6)$$

We now change variables by taking natural logarithms

$$SR(\theta, f, z) = \ln\left|\frac{A_j}{A_{wj}}\right| = \ln T_j(\theta, z) + \ln R_j(\theta, z) + \ln G_j(f, z) - \ln R_{wj}(\theta, z_w). \quad (7)$$

We note that the spectral ratio $SR$ can be readily separated into a frequency-dependent term $G$ and other, nonfrequency dependent terms, i.e.,

$$SR(\theta, f, z) = SR_0(\theta, z) + \ln G(f, z). \quad (8)$$

We also observe that

$$\ln G(f, z) = -\frac{\pi f t}{Q(z)}, \quad (9)$$

again stating that $Q$ is independent of frequency. If we fit $SR$ by least-squares into a slope and intercept, the slope becomes $(\ln G)/f$ or $(-\pi t/Q)$. The variance of the slope, therefore, becomes the variance of $(\ln G)/f$. By dividing the earth that is sampled into $n$ equally thick layers, we have for each observation $j$

$$\frac{-SR_j(f, z)}{\pi f} = \sum_{i=1}^{m} \frac{t_{ij}}{Q(z)} \quad m \leq n. \quad (10)$$

Note that the traveltime in the $i$th layer, for the $j$th observation $t_{ij}$ is a function of depth, velocities within the $i$th layer, and the apparent velocity (c.f., Dorman and Jacobson, 1981, this issue). Alternatively, we have

$$\frac{-SR_j(f, z)}{\pi f} = \sum_{i=1}^{m} k_i PL_{ij}. \quad (11)$$

Here, $PL_{ij}$ is the path length within each layer $i$, and is a function of the $j$th apparent velocity.

Numerous advantages accrue from the use of the spectral ratio method. First is the rather simple method of computation and data reduction. No spreading losses need to be calculated, because only frequency-dependent effects are examined. If reflection coefficients or scattering, for example, are frequency dependent, they will be included in the attenuation values. Thus, we will be measuring effective, rather than intrinsic attenuation. Second, our only restrictions on data collection are accurate recordings of both refracted and waterborne energy, with the source and receiver sufficiently far away from reflective boundaries to eliminate angular dependence on the source spectrum. Third, an accurate velocity depth function is needed to reduce the spectral ratio into attenuation values as a function of depth. Finally, by changing variables to logarithms, we have cast the problem as a linear one, that is, attenuation values are linearly related to the logarithm of the spectral ratio. In addition, the errors of the spectral ratio are independent of the amplitudes (Dorman, 1969). Having this linear relationship and statistical properties allow the use of classical linear inverse theory (Parker, 1977). This method (similar to least-squares analysis) allows estimates of spectral ratio variances to be incorporated into the attenuation value variance, and thus we can derive confidence limits on the attenuation depth function. Furthermore, we can trade off a smooth function with a high degree of confidence for a highly resolved attenuation function with a low level of confidence. We are primarily interested in smooth, highly confident attenuation depth functions.

The inverse technique we use is that developed by Wiggins (1972). Our system of equations is

$$\mathbf{A}\,\mathbf{b} = \mathbf{C}, \quad (12)$$

Downloaded 23 Feb 2012 to 134.246.166.168. Redistribution subject to SEG license or copyright; see Terms of Use at http://segdl.org/

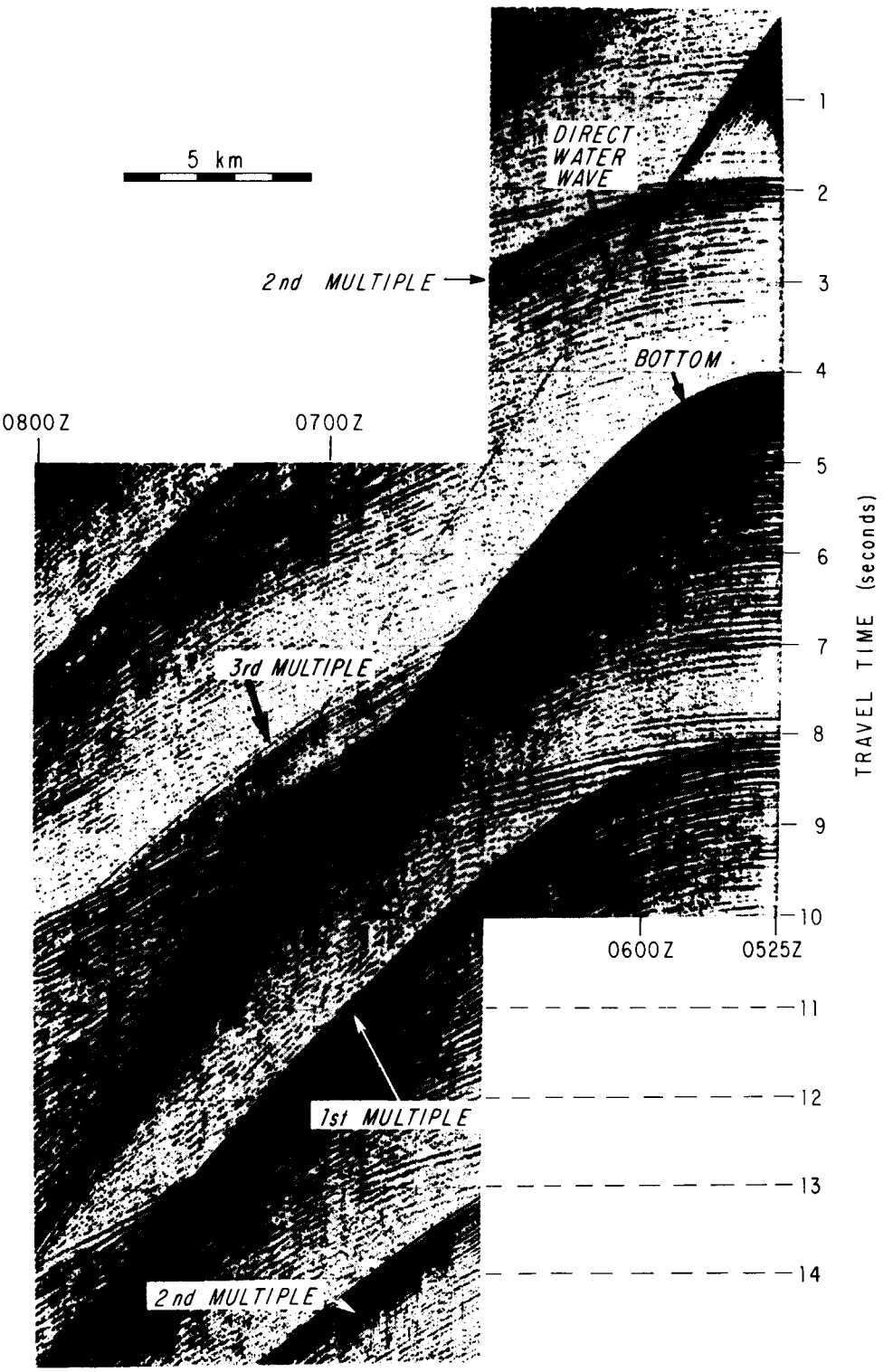


FIG. 2. Wide-angle reflection/refraction profile shot to the east at 4 knot speed. The first refracted arrivals appear at 8 sec and at approximately 0650Z time. The second set of arrivals, just before the bottom reflection, represent doubly refracted energy that has been reflected once from the top of the sedimentary section.

Downloaded 23 Feb 2012 to 134.246.166.168. Redistribution subject to SEG license or copyright; see Terms of Use at http://segdl.org/

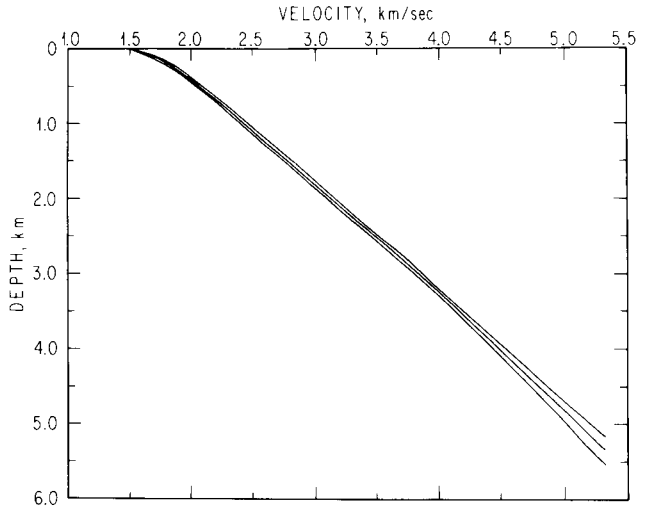


FIG. 3. The velocity-depth solution, reproduced from Dorman and Jacobson (1981), including the 98 percent (two standard deviation) confidence levels. The surface velocity of 1.503 km/sec was determined by a combination of velocity measurements on gravity cores and traveltime data.

where $A_{ij} = t_{ij}$ or $PL_{ij}$; $b_i = Q_i^{-1}$ or $k_i$; and $C_j = SR_j/(-\pi f)$ or $SR_j/(-f)$, respectively. Following Wiggins' notation **S**, the variance of **C** is the variance of the slope of the spectral ratio, and **W**, the variance of the parameters **b**, is taken to be unity. We then decompose the equations into linked orthonormal eigenvectors and rank the eigenvalues in decreasing order (Gilbert, 1971). We then take a linear combination of eigenvectors to solve the system of equations. We do this by starting with one eigenvector and incrementing the number of eigenvectors included in the solution. We select preferred solutions on the basis of chi-square analysis and correlation of the residuals of the misfits to the observational data.

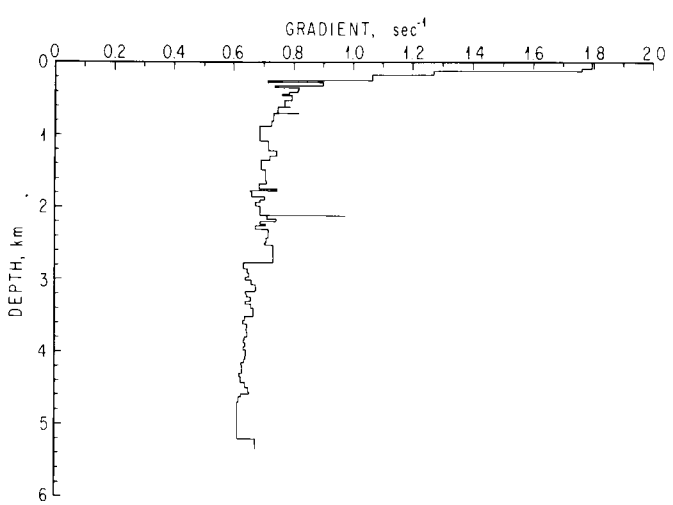


FIG. 4. The velocity gradient with depth profile, as reproduced from Dorman and Jacobson (1981). Only the best fitting solution is shown here, which was used to compute the velocity depth profile used to calculate the specific quality factor. Note in particular the rapid decrease of the gradient from 1.79 $sec^{-1}$ at the surface to 0.7 $sec^{-1}$ within 500 m.

## DATA COLLECTION

The marine seismic refraction experiment was located in the central Bay of Bengal and was conducted in February 1979. A site at 13°51′N, 88°34′E was selected for a variety of reasons. Curray and Moore (1974), Curray et al (1981), and Hamilton et al (1974, 1977) have reported that the sea floor here is composed of a section of Cenozoic terrigenously derived sediments greater than 5 km in thickness, overlying Cretaceous oceanic crust. These sediments are derived from the Himalayas, transported by the Ganges-Brahmaputra River system, and deposited on the Bengal deep sea fan. The location of the experiment is far from any major distributary channels of the fan complex, where levees and valleys introduce structure into the sea floor. The immediate area, in 3.0 km of water, was extremely flat (Figure 1), simplifying some of the data reduction. Most important, however, was the lack of sediment velocity discontinuities. Hamilton et al (1974, 1977) predict a smooth increase of velocity with depth.

To measure attenuation accurately, energy that refracts entirely through the sediments must be observed without interference from energy traveling along other paths. This requires placing both receivers and sources as close to the sea floor as possible. Use of SUS Mk94 mod 0 depth charges (Naval Ordnance Systems Command, 1973) set to 6000 or 8000 ft (1829 or 2438 m) together with either 256 lb of TNT or 240 lb of HBX enabled a deep, broadband frequency source, independent of the angle of inclination of propagation. Since the shot instants for these depth charges are not as predictable as for near-surface charges, an event triggered microprocessor-controlled, digitally recording, sea floor hydrophone system was used as the receiver. Two of these instruments were deployed on the ocean floor approximately 250 m apart. (We later discuss the effect of using sea floor receivers on the angular dependence of monitoring the source function.) The sampling interval was 5 msec. With an antialias filter, signals with frequency content up to 80 Hz could be recorded reliably. Total dynamic range of the instrument is 132 dB, with a resolution of 72 dB. All data were stored in memory before being transferred to magnetic tape, eliminating introduction of mechanical vibration from tape transport into the recorded signal.

A moored, near-surface, telemetering hydrophone buoy (Buoy Jo) was also deployed near the sea floor hydrophones (Figure 1). This unit was used for wide angle reflection/refraction measurements (Figure 2). The telemetered signals for the air gun refraction work were digitized at 128 Hz after being sent through the antialias filter with a corner frequency of 32 Hz. Use of the ship's 3.5-kHz echosounder and Buoy Jo enabled an analog ranging system to be used out to about 15 km.

The refraction profile was a combination of two outgoing lines. All deep charges were deployed as the ship drifted southwestward at a steady 0.8 knots. Use of the ranging system enabled deploying the charges at 250- or 500-m intervals at 8- or 17-minute intervals. Several shots did not fire, and the line was reshot at 4 knots speed to the south to fill in the gaps in data.

## THE VELOCITY-DEPTH FUNCTION

Because of the interdependence of attenuation and velocity structure in determining the specific factor $Q^{-1}$, it was essential to describe an adequate velocity depth function. Because of the apparently smooth increase of velocity with distance (Figure 2) and thus with depth, it was felt that a model with planar homogenous layers (Ewing, 1963; Officer, 1958) would make an inadequate description. A better solution is to assume linear velocity gradients

Downloaded 23 Feb 2012 to 134.246.166.168. Redistribution subject to SEG license or copyright; see Terms of Use at http://segdl.org/

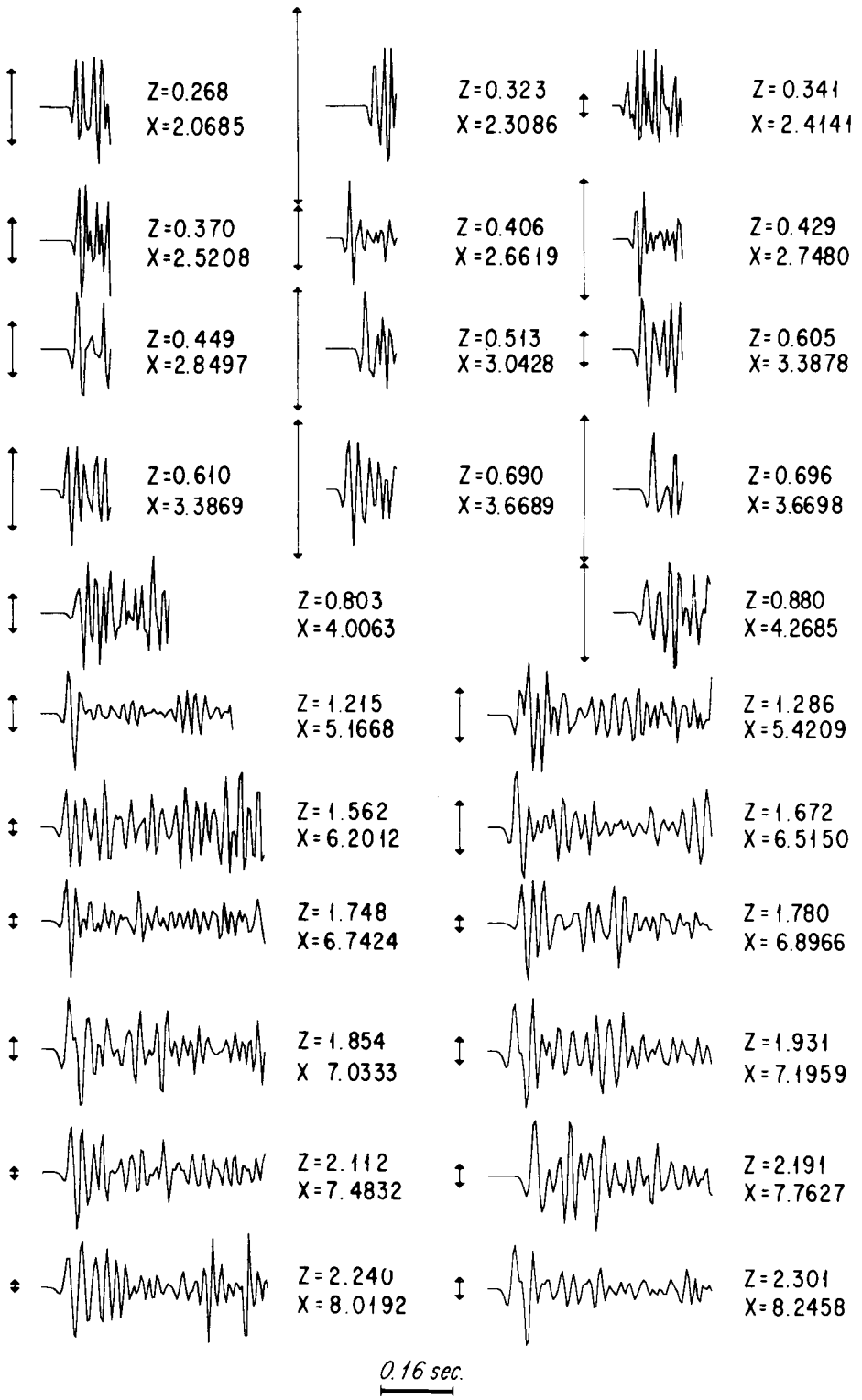


FIG. 5. Autoscaled plots of the refracted energy used in determining spectral ratios. Each plot begins at the 0.16-sec time window used in the analysis. Vertical lines represent the maximum peak-to-peak amplitude of the wavelet before autoscaling. Hydrophone responses have been approximately adjusted to be equal for this figure. The complex nature of most of these waves probably results from fine scale multipathing within the sedimentary column. Positive pressure is downward.

Downloaded 23 Feb 2012 to 134.246.166.168. Redistribution subject to SEG license or copyright; see Terms of Use at http://segdl.org/

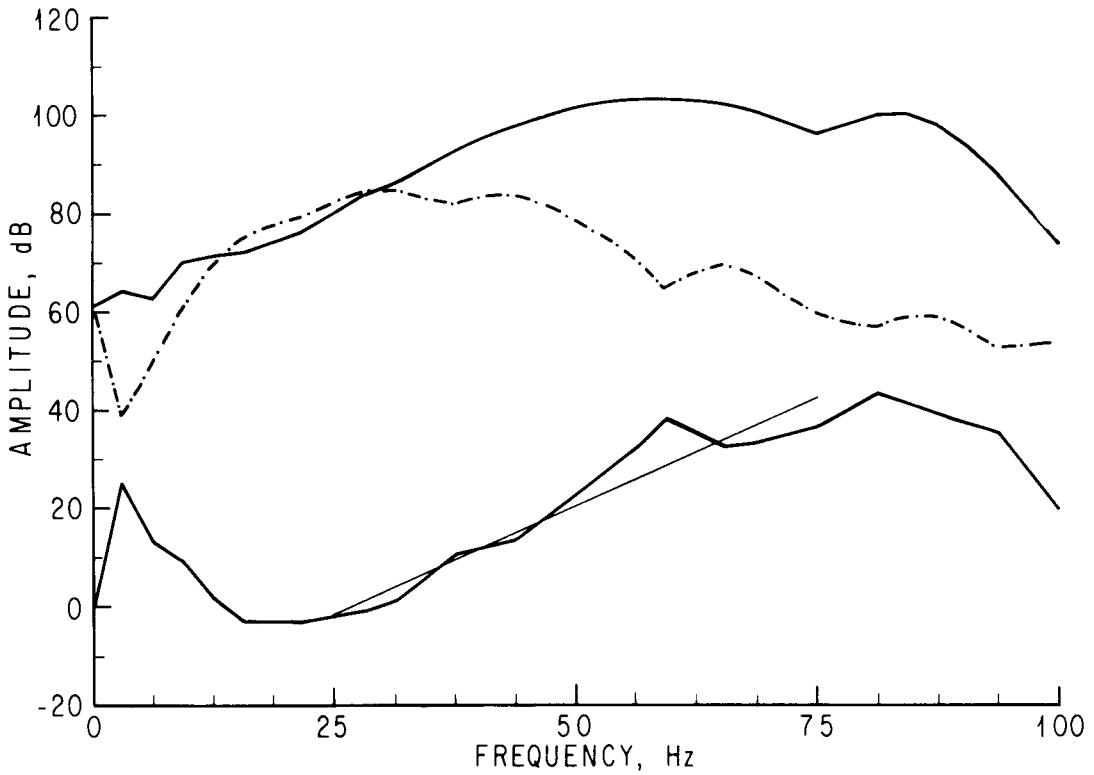


FIG. 6. The unwindowed spectrum of the direct waterborne path (solid upper line) and the refracted arrival (dashed line) for the wave penetrating to 1.215-km depth. The lower solid line is the spectral ratio of the direct arrival to the refracted arrival, showing the least-squares slope, fit between 25 to 75 Hz. The slope was determined to be 1.097 ± 0.033 dB/Hz. This figure represents the best quality fit of all the spectral ratios. The average variance of the slopes was 0.21 dB/Hz.

with depth, as Dorman (1979) and Dorman and Jacobson (1981) have discussed.

The first step in inverting the traveltime data into a velocity-depth function is to reduce all the data to the sea floor. The reduced traveltime data consist of the combination of deep charges, recorded by the sea floor hydrophones, and refractions recorded by Buoy Jo (Figure 2) from air gun sources. A fourth-order polynomial of distance versus time was then performed on the traveltime data, in order to derive the apparent velocity for each arrival. This apparent velocity is the derivative of the regression at each observation. Two adjustments, however, were made to the polynomial regression. The first condition was that the traveltime curve pass through the origin. The second adjustment was made for the slope at the origin, or the initial velocity at the sea floor. Velocity analysis of water-saturated cores, taken within 2 km of the station (Figure 1), were performed. The cores, consisting of silty clays, were divided into 10-cm sections, and velocities were calculated using the method of Hamilton (1970). The average in-situ core velocity was 1.4865 km/sec, with a standard deviation of 0.0121 km/sec. These values were introduced into the polynomial regression as an additional observation. The regression then determined that 1.503 km/sec was the least-squares estimate of the sea floor velocity.

Once the apparent velocities were determined, the traveltime data were reparameterized into tau and zeta, defined as follows:

$$\tau = T - px, \tag{13a}$$

and

$$\zeta = T + px, \tag{13b}$$

where $T$ is traveltime, $x$ is the range, and $p$ is the apparent slowness (or inverse velocity) that the wave travels. Tau and zeta are orthonormal pairs and thus have statistically independent errors (Dorman and Jacobson, 1981). These values are linearly related to dZ/dv, or the inverse velocity gradient. The singular value decomposition method of Wiggins (1972) was used to solve for the inverse velocity gradient as a function of slowness. This function was integrated, knowing the velocity, to give the velocity depth function. The reader is referred to Dorman and Jacobson (1981) for a more complete discussion of this inversion technique. The solution of the velocity depth function, shown in Figure 3, depicts the least-squares fit and the 98 percent (two sigma) confidence bounds. As can be seen, velocity increases smoothly up to 5 km of depth. The section of sediments is much thicker than 5 km, possibly up to 8 km (Curray et al, 1981). The velocity gradient solution shown in Figure 4 shows the rapid decrease of the gradient to about 400 m; thereafter, the velocity gradient is reasonably constant at 0.6 to 0.7 $sec^{-1}$, similar to values discussed by Bachman and Hamilton (1980) in the Arabian fan, an analogous deep sea fan. The initial gradient of 1.795 $sec^{-1}$ is pleasingly close to the value of 1.87 $sec^{-1}$ that Hamilton et al (1977) predict for the central Bay of Bengal, based on sonobuoy wide-angle reflection measurements (e.g., Le Pichon et al 1968).

## THE ATTENUATION DEPTH FUNCTION

The data used for determining spectral ratios were taken only from the sea floor hydrophones. The Buoy Jo data were not used for a number of reasons: the signal-to-noise (S/N) ratio was poor due to multiples (Figure 2); the bandwidth of usable signal was small and the source (air guns) were near surface, making the spec-

Downloaded 23 Feb 2012 to 134.246.166.168. Redistribution subject to SEG license or copyright; see Terms of Use at http://segdl.org/

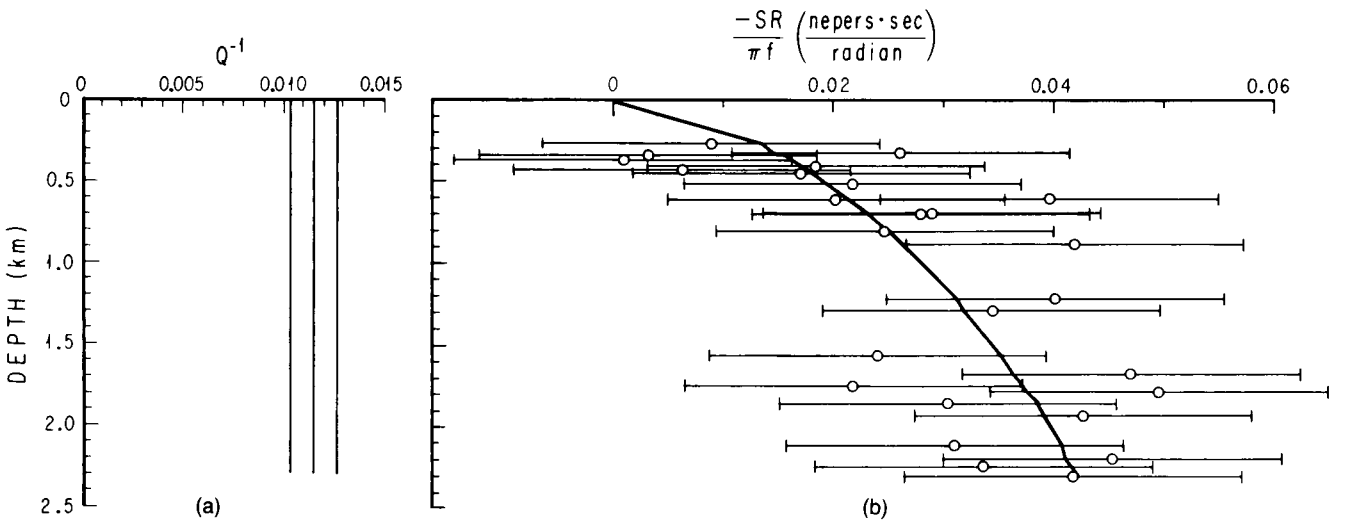


FIG. 7. The constant specific quality factor $Q^{-1}$ solution and the fit to the data. The number of observations is 26 and the chi-square fit for this solution is 38.80. The value of $Q$ is 86.92, corresponding to a value of 0.0115 for $Q^{-1}$

trum of the source dependent upon the angle of inclination or the apparent velocity.

Before describing the attenuation solutions, we should first mention some of the problems we had in recording the signals. Upon recovery of the instruments at sea, we discovered that one hydrophone had leaked, and its response dropped by approximately 40 dB. This turned out to be fortunate, however, for the other instrument's recording was found to be clipped for the direct water wave arrival. Thus, we were forced to use the water wave signal received by the bad hydrophone for our source function. We could only calibrate this hydrophone over part of the frequencies of interest. The frequency response curve was similar to the other hydrophone's response but offset by 40 dB. A further problem encountered was that the antialias filter was driven into its range of nonlinear response. We were then forced to assume that the nonlinear response was insignificant. As we shall see, our results are fairly consistent, indicating this assumption is tolerable.

We mentioned earlier that for a reliable measurement of the source function, the source and receiver need to be away from reflective boundaries. The sea floor hydrophones, being about 2 m above the sea floor, do not satisfy this criterion. For each reception of the direct path signal, we should see three other signals traveling along other paths that contaminate the signal in which we are interested. These other paths include a reflection off the sea floor, a shallow refracted arrival, and possible contamination by the deeply refracted arrival. To investigate this problem, we compared the spectrum of our direct water signal with two other spectra of waterborne signals reflected from the sea surface. We found the shape of the spectral curves differed only slightly in shape, indicating that the multipathing problem is insignificant. It would still be preferable to have a second receiver to measure the source signal, that is far from both the bottom and surface of the water column.

In order not to contaminate our received signals with other energy traveling along different paths, visual inspection of the records allowed a selection of a time window of 160 msec (32 samples) for each first refracted arrival, and for the direct water wave for the instrument with the reduced response. The 26 observations of refracted energy are depicted in Figure 5. A fast Fourier transform was computed, and spectral ratios were calculated (Figure 6). Signal-to-noise ratios ranged from 55 to 90 dB for the refracted arrivals, and from 20 dB to 70 dB for the direct arrival. For the shot depth and weight used, the dominant frequencies should lie within the 50 to 60 Hz band. However, each water wave spectrum showed that the dominant frequency was above 80 Hz, indicating either partial detonation or nonlinear responses of the filters.

The value of the slope of the spectral ratio used for determining $Q^{-1}$ [equation (10)] was determined by least squares from 25 to 75 Hz. The standard deviation of the slope was then used to compute the variance of each observation. Variances of the observations ranged widely. Even for the same shot, each of the two observations has variances sometimes differing by an order of magnitude. In fact, in two cases where waves from different shots penetrated to the same depth, observations and variances differed considerably. We feel that this is a result of small-scale multipathing within the sediments, as Schoenberger and Levin (1974, 1978, 1979) have reported. Since we wish to reduce the dependence of multipathing on variance (and thus reduce any biasing of the data), we averaged all the variances to get a more stable estimate.

One of our assumptions was that the spectral ratio can be described as only a function of frequency to the first power. Given the fact that the observed average variance of the term for the first power of frequency was high, it was felt that it would be futile to test for higher-order terms of frequency components of the spectral ratio.

As mentioned before, one of the great advantages of linear inverse theory is the ability to solve in a least-squares sense an infinity of models. The disadvantage is that there is no one best solution, so that solutions that are preferred are chosen on the basis of subjective judgment. We solve for the specific quality factor $Q^{-1}$ first, and later determine the attenuation coefficient $k$ in order to compare our data to that predicted by Hamilton (1976a).

We first cast the inversion problem to solve for constant $Q^{-1}$. Figure 7a, b shows this function, the 98 percent confidence regions (two standard deviations), and the corresponding fit to the data. The value for $Q^{-1}$ is 0.0115 with a chi-square of 38.80 with 26 observations. As one can see in Figure 7b, the fit to the data of a constant $Q^{-1}$ model is not bad, considering the scatter in the data and the rather large error bounds. This value of $Q^{-1}$ was used to compute the amount of velocity dispersion over the frequencies of

Downloaded 23 Feb 2012 to 134.246.166.168. Redistribution subject to SEG license or copyright; see Terms of Use at http://segdl.org/

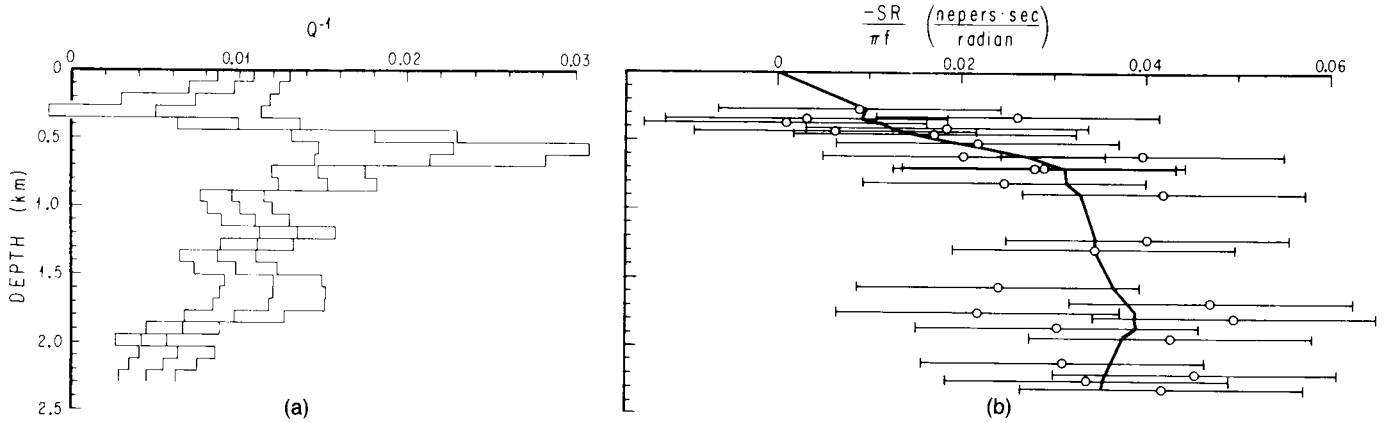


FIG. 8. The preferred solution for $Q^{-1}$ as a function of depth. Chi square is equal to 30.86.

interest (25 to 75 Hz), using the relationship proposed by Kanamori and Anderson (1977). The dispersion amounted to only 0.4 percent, well within experimental errors.

To get a more detailed solution of attenuation as a function of depth, it was necessary to divide the section into equally thick layers. The reason for this lies in nonuniform data spacing. If we had chosen the layer thickness to be defined by the separation of the data in depth, we would have to tailor the a priori parameter variance **W** to produce smooth eigenvectors that are independent of layer thickness. We do not always know how to do this. Since we are interested in highly smooth functions, we arbitrarily chose 26 equally thick layers. After looking at many different solutions (some with negative $Q^{-1}$), we selected the profile shown in Figure 8a. Here, only three eigenvectors were retained, providing a fairly smooth attenuation function with a high degree of statistical confidence, with a chi-square of 30.86. Notice that the 98 percent confidence bounds of $Q^{-1}$ extend beyond zero at 300-m depth. Figure 8b shows how the solution fits the observations. Although there is some variability in the attenuation depth function, some observations can be made. The specific quality factor $Q^{-1}$ first decreases to about 350-m depth, then increases to a maximum, then decreases, and thereafter remains fairly constant deeper in the section (Figure 8a).

We also inverted the spectral ratio observations to determine the attenuation coefficient $k$ versus depth. We first solved for constant $k$, which yielded a value of 0.13 dB/m/kHz, with chi-square of 47.58. We felt that this value of chi-square was too high, and thus a constant $k$ solution was inadequate to describe the data. Figure 9a, b shows a preferred solution, retaining four eigenvectors, and having a chi-square of 29.70. With this particular solution, a peak of attenuation coefficient of 0.29 dB/m/kHz is evident at 600-m depth, decreasing to about 0.10 dB/m/kHz at greater depths. This profile shows that our data are reasonably consistent with the model of Hamilton (1976a). Two distinguishing differences exist between our data and Hamilton's compilation. First, we find that the attenuation coefficient remains essentially constant to about 350-m depth. Although we do not have many data at this shallow depth, nearly all solutions with four or more eigenvectors show this common feature of constant attenuation. Second, attenuation coefficient values do not decrease to 0.02 dB/m/kHz at 2-km depth as

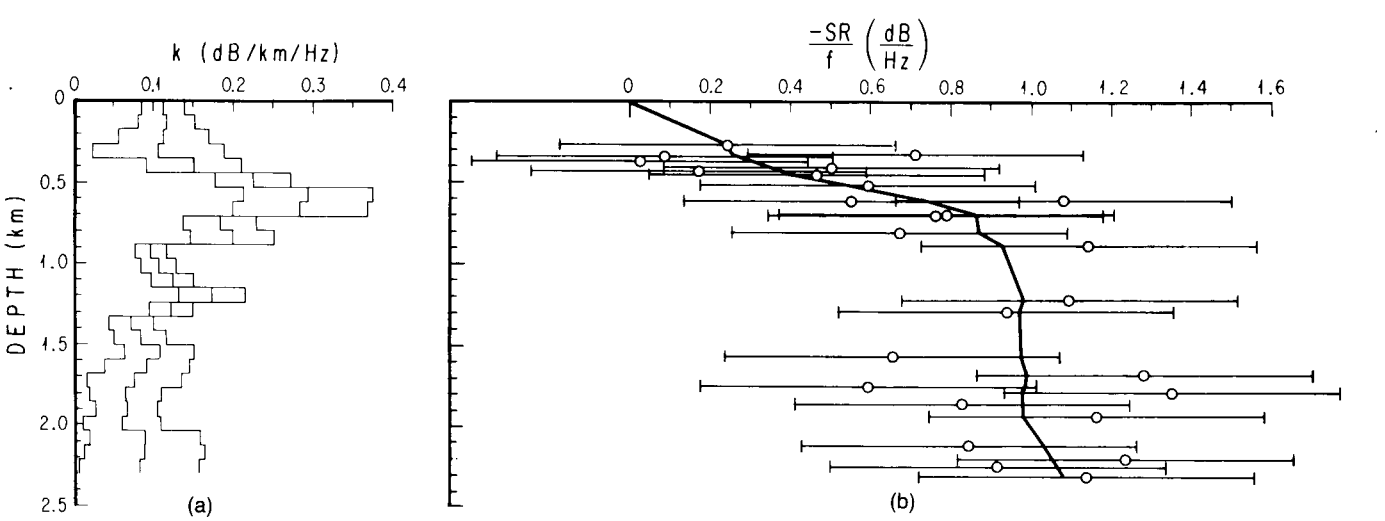


FIG. 9. The preferred solution for attenuation coefficient $k$ and the fit to the data. Here, the chi-square value is 29.70.

Downloaded 23 Feb 2012 to 134.246.166.168. Redistribution subject to SEG license or copyright; see Terms of Use at http://segdl.org/

Hamilton predicts. Rather, the attenuation varies somewhat about the value of 0.10 dB/m/kHz below 0.8 km with a slight decrease with depth.

## DISCUSSION

As mentioned earlier, attenuation coefficient $k$ and specific quality factor $Q^{-1}$ are not exactly equivalent. Although they each describe some measure of attenuation, the relationship between the two is

$$8.686 \frac{\pi t}{Q} = kPL. \tag{14}$$

But the path length $PL$ is related to traveltime by the velocity, i.e., by using differential traveltimes and path lengths

$$dPL = Vdt. \tag{15}$$

Thus, $\pi/Q$ is proportonal to $kV$.

Let us now look at the equivalent representation of $Q^{-1}$ in terms of Hamilton's (1976) attenuation coefficient. Figure 10 represents the smoothed version of our attenuation coefficient model as a function of depth. When we transform this model in terms of $Q^{-1}$, the result is Figure 10b. Here $Q^{-1}$ increases (due to increasing velocity) while $k$ remains constant at shallow depths. At the peak of the attenuation coefficient with depth, the specific quality factor $Q^{-1}$ reaches its maximum value. At still deeper depths, $k$ decreases, while $Q^{-1}$ remains constant. We now seem to have a paradox. In one case ($k$), attenuation reaches a peak, and then decreases with depth. In the other case ($Q^{-1}$), attenuation increases to a maximum, decreases rapidly, and then remains constant with depth. The key to this puzzle lies in the units of measure and the relationship to depth. The attenuation coefficient measures attenuation relative to the unit of length, while $Q^{-1}$ measures absorption of a cycle of energy. As energy proceeds deeper into the sedimentary section, the wavelength increases, and thus a unit of length becomes a smaller portion of a wavelength.

We feel that attenuation is best described as a measure of energy loss per unit cycle. This measure is independent of frequency and velocity, unlike the attenuation coefficient. Hamilton's explanation for the decrease of the attenuation coefficient, i.e., the overburden pressure on the frame structure, is not the dominant factor. Rather, we suggest, the dominant reason for the decrease of $k$ values is the increase of velocity with depth.

A remaining question is: How does attenuation vary at shallow depths? Our data indicate that $Q^{-1}$ decreases with depth. Because of the relationship with depth, this would imply that attenuation coefficient $k$ would also decrease with depth, which is not the case (Figure 9). It is important to point out that our data do not adequately constrain these attenuation depth relationships at depths less than 300 m. Hamilton (1976a) predicts the attenuation coefficient would increase due to porosity reductions with depth. Reducing the porosity causes a more densely packed sediment structure. Consequently, there are more intergranular contacts, which have the effect of increasing attenuation (Hamilton, 1972). Unfortunately, there are no published data regarding the effect of porosity reductions with depth on attenuation for unlithified marine sediments (Hamilton, personal communication, 1980). Other factors which may affect the shallow attenuation values we observe include lithologic changes, grain size changes, and the possible presence of gas in the interstitial water.

We now wish to address ourselves to a discussion of the peak of attenuation at 500 to 700 m depth. Both methods of describing attenuation reveal this peak, although it seems to be more pronounced in the specific quality factor model (Figure 8). Hamilton (1976a) predicts this peak to occur at 200 to 300 m depth, due to the countering effects of porosity reduction and overburden pressure effects.

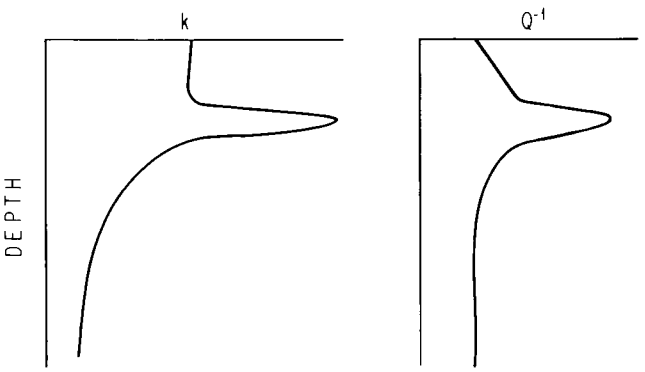


FIG. 10. Equivalent representations of the specific quality factor $Q^{-1}$ and the attenuation coefficient $k$ for a very smoothed version of the attenuation depth profile for our data.

The observed depth, at approximately 600 m, is close to the depth at which induration becomes complete and the unlithified sediment becomes a mudstone. Hamilton (1976b) reports depths of 590 m in the Arabian fan and 450 m in the Somali basin as depths of lithification. He also describes a peak of rebound of porosity at 600-m depth, which he describes as being the boundary between lithified and unlithified sediments. This is also the depth where the velocity gradient curve reaches its nominal value of 0.65 $sec^{-1}$ (Figure 4). We feel that the observed peak of attenuation at 600-m depth is a consequence of sediment lithification and must be related to the collapse of the cardhouse structure of the unlithified sediment (Hamilton, 1970). The collapse of the mineral structure, once consisting of randomly oriented clay and silt particles, would produce subparallel layering of mineral grains, which might explain observed velocity anisotropy in marine sediments (Bachman, 1979). The rapid increase of intergranular contacts could explain the increase of attenuation at the 500 to 600 m depth. The rapid decrease of attenuation at slightly deeper depths can be explained by cementation of mineral grains, reducing the sliding friction that seems to be the dominant mechanism for attenuation.

A possible alternative explanation for the peak of attenuation is the presence of a primarily sandy layer at this depth. Without a deep core nearby, we cannot distinguish between the two possibilities. We prefer the explanation of lithification for the increase of attenuation. If this explanation is correct, we now have two methods of determining the depth of lithification: the inflection in the velocity gradient depth curve and the pronounced peak of attenuation.

The possibility of lithologic changes can and probably do manifest themselves in attenuation depth profiles. Many of the secondary peaks in the specific quality factor profile (Figure 9) can be due to a sandier constituency. We still do not completely understand the effects of porosity, lithification, sediment type, and sedimentation rate on attenuation depth profiles. Only when more profiles are made and better laboratory work is performed can we perhaps clarify these relationships.

Downloaded 23 Feb 2012 to 134.246.166.168. Redistribution subject to SEG license or copyright; see Terms of Use at http://segdl.org/

## ACKNOWLEDGMENTS

We wish to thank the master and crew of the *R/V Thomas Washington* for their cooperation and assistance. Special thanks are extended to Ed Hamilton, Dick Bachman, and Bob Wallace of the Naval Ocean Systems Center for their help in analyzing the sediment cores.

This work was supported by NORDA contract number N00014-75-C-0749, N00014-80-C-0219 to the Marine Physical Laboratory and by ONR contract N00014-75-C-0152 (Code 480) to the Geological Research Division.

Contribution of the Scripps Institution of Oceanography, new series.

## REFERENCES

Bachman, R. T., 1979, Acoustic anisotropy in marine sediments and sedimentary rocks: J. Geophys. Res., v. 84, p. 7661–7663.

Bachman, R. T., and Hamilton, E. L., 1980, Sediment sound velocities from sonobuoys, Arabian Fan: J. Geophys. Res. v. 85, p. 849–852.

Curray, J. R., and Moore, D. G., 1974, Sedimentary and tectonic processes in the Bengal Deep-Sea Fan and geosyncline, *in* Continental margins: C. A. Burk and C. L. Drake, Ed., New York, Springer-Verlag, p. 617–627.

Curray, J. R., Emmel, F. J., Moore, D. G., and Raitt, R. W., 1981, Structure, tectonics and geological history of the northeastern Indian Ocean, *in* The ocean basins and margins, v. 6: A. E. N. Nairn and F. G. Stehli, Ed., New York, Plenum Press.

Dorman, L. M., 1968, Anelasticity and the spectra of body waves: J. Geophys. Res., v. 73, p. 3877–3883.

——— 1969, Reply to J.-C. De Bremaecher's comment on "Anelasticity and the spectra of body waves": J. Geophys. Res., v. 74, p. 3304–3307.

——— 1979, A linear relationship between Earth models and seismic body wave data: Geophys, Res. Lett. v. 6, p. 132–134.

Dorman, L. M., and Jacobson, R. S., 1981, Linear inversion of body wave data, Part I: Velocity structure from traveltimes and ranges: Geophysics, v. 46, this issue, p. 138–151.

Ewing, J. I., 1963, Elementary theory of seismic refraction and reflection measurements, *in* The sea, v. 3: M. N. Hill, Ed., New York, Interscience, p. 3–19.

Gilbert, F., 1971, Ranking and winnowing gross Earth data for inversion and resolution: Geophys. J. Roy Astr. Soc., v. 23, p. 125–128.

Hamilton, E. L., 1970, Sound velocity and related properties of marine sediments, North Pacific: J. Geophys. Res., v. 75, p. 4423–4446.

——— 1972, Compressional-wave attenuation in marine sediments: Geophysics, v. 37, p. 620–646.

——— 1976a, Sound attenuation as a function of depth in the sea floor: J. Acoust. Soc. Am., v. 59, p. 528–535.

——— 1976b, Variations of density and porosity with depth in deep-sea sediments: J. Sed. Petrol., v. 46, p. 280–300.

Hamilton, E. L., Moore, D. G., Buffington, E. C., Sherrer, P. L., and Curray, J. R., 1974, Sediment velocities from sonobuoys: Bay of Bengal, Bering Sea, Japan Sea and North Pacific: J. Geophys. Res., v. 79, p. 2653–2668.

Hamilton, E. L., Bachman, R. T., Curray, J. R., and Moore, D. G., 1977, Sediment velocities from sonobuoys: Bengal Fan, Sunda Trench, Andaman Basin and Nicobar Fan: J. Geophys. Res., v. 82, p. 3003–3012.

Jeffreys, H., 1965, Damping of *S* waves: Nature, v. 208, p. 675.

Kanamori, H., and Anderson, D. L., 1977, Importance of physical dispersion in surface wave and free oscillation problems, review: Rev. Geophys. Space Phys., v. 15, p. 105–112.

Le Pichon, X., Ewing, J., and Houtz, R. F., 1968, Deep-sea sediment velocity determination made while reflection profiling: J. Geophys. Res. v. 73, p. 2597–2614.

Mitchell, S. K., and Focke, K. C., 1980, New measurements of compressional wave attenuation in deep ocean sediments: J. Acoust. Soc. Am., v. 67, p. 1582–1589.

Naval Ordnance Systems Command, 1973, NAVORD OP3696, Technical Manual, Explosives safety precautions for research vessels.

Officer, C. B., 1958, Introduction to the theory of sound transmission: New York, McGraw-Hill Book Co., Inc.

Parker, R. L., 1977, Understanding inverse theory: Ann. Rev. Earth Planet. Sci., v. 5, p. 35–64.

Schoenberger, M., and Levin, F. K., 1974, Apparent attenuation due to intrabed multiples: Geophysics, v. 39, p. 278–291.

——— 1978, Apparent attenuation due to intrabed multiples, II: Geophysics, v. 43, p. 730–737.

——— 1979, The effect of subsurface sampling on 1-D synthetic seismograms: Geophysics, v. 44, p. 1813–1829.

Urick, R. J., 1975, Principles of underwater sound, 2nd ed.: New York, McGraw-Hill Book Co., Inc.

Wiggins, R. A., 1972, The general linear inverse problem: Implication of surface waves and free oscillations for earth structure: Rev. Geophys. Space Physics, v. 10, p. 251–285.

Downloaded 23 Feb 2012 to 134.246.166.168. Redistribution subject to SEG license or copyright; see Terms of Use at http://segdl.org/